

## Deuterium fractionation as a multi-phase component tracer in the Galactic Centre

LAURA COLZI,<sup>1,2</sup> JESÚS MARTÍN-PINTADO,<sup>1</sup> VÍCTOR M. RIVILLA,<sup>1,2</sup> IZASKUN JIMÉNEZ-SERRA,<sup>1</sup> SHAOSHAN ZENG,<sup>3</sup>  
LUCAS F. RODRÍGUEZ-ALMEIDA,<sup>1</sup> FERNANDO RICO-VILLAS,<sup>1</sup> SERGIO MARTÍN,<sup>4,5</sup> AND MIGUEL A. REQUENA-TORRES<sup>6,7</sup>

<sup>1</sup>*Centro de Astrobiología (CSIC-INTA), Ctra. de Ajalvir Km. 4, 28850, Torrejón de Ardoz, Madrid, Spain*

<sup>2</sup>*INAF-Osservatorio Astrofisico di Arcetri, Largo E. Fermi 5, I-50125, Florence, Italy*

<sup>3</sup>*Star and Planet Formation Laboratory, Cluster for Pioneering Research, RIKEN, 2-1 Hirosawa, Wako, Saitama, 351-0198, Japan*

<sup>4</sup>*European Southern Observatory, Alonso de Córdova, 3107, Vitacura, Santiago 763-0355, Chile*

<sup>5</sup>*Joint ALMA Observatory, Alonso de Córdova, 3107, Vitacura, Santiago 763-0355, Chile*

<sup>6</sup>*University of Maryland, College Park, MD 20742-2421, USA*

<sup>7</sup>*Department of Physics, Astronomy and Geosciences, Towson University, MD 21252, USA*

### ABSTRACT

The Central Molecular Zone (CMZ) contains most of the mass of our Galaxy but its star formation rate is one order of magnitude lower than in the Galactic disc. This is likely related to the fact that the bulk of the gas in the CMZ is in a warm ( $>100$  K) and turbulent phase with little material in the pre-stellar phase. We present in this Letter observations of deuterium fractionation (D/H ratios) of HCN, HNC, HCO<sup>+</sup>, and N<sub>2</sub>H<sup>+</sup> towards the CMZ molecular cloud G+0.693-0.027. These observations clearly show, for the first time, the presence of a colder, denser, and less turbulent narrow component, with a line width of  $\sim 9$  km s<sup>-1</sup>, in addition to the warm, less dense and turbulent broad component with a line width of  $\sim 20$  km s<sup>-1</sup>. The very low D/H ratio  $\leq 6 \times 10^{-5}$  for HCO<sup>+</sup> and N<sub>2</sub>H<sup>+</sup>, close to the cosmic value ( $\sim 2.5 \times 10^{-5}$ ), and the high D/H ratios  $> 4 \times 10^{-4}$  for HCN and HNC derived for the broad component, confirm the presence of high-temperatures deuteration routes for nitriles. For the narrow component we have derived D/H ratios  $> 10^{-4}$  and excitation temperatures of 7 K for all molecules, suggesting kinetic temperatures  $\leq 30$  K and H<sub>2</sub> densities  $\geq 5 \times 10^4$  cm<sup>-3</sup>, at least one order of magnitude larger than for the broad component. The method presented in this Letter allows to identify clouds on the verge of star formation, i.e. under pre-stellar conditions, towards the CMZ. This method can also be used for the identification of such clouds in external galaxies.

*Keywords:* Interstellar molecules - Isotopic abundances - Galactic Center - Star formation

### 1. INTRODUCTION

The inner 500 pc of our Galaxy, known as the Central Molecular Zone (CMZ), contains  $\sim 80\%$  of the dense ( $>10^4$  cm<sup>-3</sup>) molecular gas in the Galaxy ( $M_{\text{CMZ}}=2-6 \times 10^7 M_{\odot}$ ; Morris & Serabyn 1996). However, despite this large reservoir of matter, the star formation rate in the CMZ is at least one order of magnitude lower than in the Disc (Longmore et al. 2013; Barnes et al. 2017).

Even if this harsh environment is able to inhibit star formation, it does not stop it completely, and some star formation activity is taking place in the CMZ, as

seen from the Arches and Quintuplet clusters, and the younger protoclusters in the Sgr B2 region. The reasons for the suppression of star formation in the CMZ are still not fully understood but are related with its extreme environmental conditions that provide additional support against gravitational collapse (e.g. Morris & Serabyn 1996). In particular, the high level of turbulence due to large internal cloud velocity dispersion ( $\sim 15-50$  km s<sup>-1</sup>, Morris & Serabyn 1996) and widespread high kinetic temperatures ( $T$  from  $\sim 50$  K to  $>100$  K, Guesten & Ungerechts 1985; Huettmeister et al. 1993; Ginsburg et al. 2016; Krieger et al. 2017) could prevent star formation. In order to understand how star formation proceeds in the CMZ, it is crucial to identify and study the earlier evolutionary stages of the dense, cold and quiescent pre-stellar cores. In principle, one expects that for pre-stellar

cores to be formed, enough energy (turbulence) has to be dissipated so that gravitational collapse can proceed. Therefore, it is foreseen that pre-stellar cores in the CMZ also present narrower line emission than its surrounding turbulent gas. So far, only one progenitor of protocluster in the CMZ have been proposed, the G0.253+0.016 molecular cloud, aka "the brick", which already shows all signposts of massive star formation (Longmore et al. 2012). However, it is still not clear whether the lack of detection of starless clouds at very early evolutionary stages is directly related to an observational bias. This is due to the presence of warm layers (or envelopes) with large column densities and high velocity dispersion making difficult to observationally disentangle the signatures of the denser and less turbulent pre-stellar gas.

Observation of deuterated molecules is a powerful tool to follow the history of the cold pre-stellar phase of star formation (Caselli & Ceccarelli 2012), both in low-mass and high-mass star-forming regions (e.g. Crapsi et al. 2005; Caselli et al. 2008; Emprechtinger et al. 2009; Fontani et al. 2011). The high densities ( $n > 10^5 \text{ cm}^{-3}$ ) and low temperatures ( $T \leq 30 \text{ K}$ ) of pre-stellar phases enhance the gas-phase abundance of  $\text{H}_3^+$ , since its main destroying agent, CO, depletes onto the surface of dust grains. The reaction of  $\text{H}_3^+$  with HD (the main reservoir of D in the ISM) produces  $\text{H}_2\text{D}^+$ , which transfers D to other species. As a result, deuterium fractionation in molecules is known to increase their abundance by several orders of magnitude above the D primordial value,  $\text{D}/\text{H} = (2.55 \pm 0.03) \times 10^{-5}$  (Zavarygin et al. 2018).

In this Letter, we illustrate how the deuterium fractionation of molecules (D/H ratio) traces the pre-stellar component embedded in massive warm and turbulent envelopes in the CMZ. We present observations of deuterated species of HCN, HNC,  $\text{HCO}^+$  and  $\text{N}_2\text{H}^+$  towards the warm and highly turbulent molecular cloud G+0.693–0.027 (hereafter G+0.693), located in the Sgr B2 complex. In particular, Sgr B2 consists of three main sources, Sgr B2(North), Sgr B2(Main), and Sgr B2(South), which are positioned along a north–south ridge. Since Sgr B2(N) is at an earlier stage of star formation than Sgr B2(M) (e.g. de Vicente et al. 2000), it seems the star formation activity occurs sequentially from the center to the north. If this is the case, early star formation activity is also expected towards G+0.693 since it is located  $\sim 55$  arcsec northeast from Sgr B2(N). However, G+0.693 does not show any signposts of ongoing star formation such as ultracompact HII regions,  $\text{H}_2\text{O}$  masers, or dust continuum point sources (Ginsburg et al. 2018). A recent study of gas morphology and kinematics in this region (Zeng et al. 2020) suggests this cloud to be affected by a cloud-cloud collision pro-

ducing the shocks likely responsible for its rich chemistry due the sputtering of molecules from dust grains (e.g. Martín et al. 2008; Requena-Torres et al. 2006; Zeng et al. 2018; Rivilla et al. 2019; Rivilla et al. 2020; Jiménez-Serra et al. 2020; Rivilla et al. 2021). In addition to the turbulent gas component (line widths  $\geq 15\text{--}30 \text{ km s}^{-1}$ ), with a density of about  $10^4 \text{ cm}^{-3}$  and a gas temperature  $> 100 \text{ K}$  (e.g. Zeng et al. 2018; Zeng et al. 2020), usually observed in the CMZ, the observed deuterated molecules pinpoint a new component with denser ( $n \geq 5 \times 10^4 \text{ cm}^{-3}$ ), colder ( $T \leq 30 \text{ K}$ ) and less turbulent (line widths  $\sim 9 \text{ km s}^{-1}$ ) molecular gas component (pre-stellar) in the CMZ, which might be on the verge of gravitational collapse. Deuterated species can thus be used as key tracers to disentangle the multi-phase components in the CMZ, and reveal the location and physical conditions of cores where the next generation of stellar clusters will form.

## 2. OBSERVATIONS

The data presented in this work was taken from the high-sensitivity spectral survey towards the G+0.693 molecular cloud (e.g. Rodríguez-Almeida et al. 2021a,b; Rivilla et al. 2021; Zeng et al. 2021) carried out with the IRAM 30m (Granada, Spain) and APEX (Chajnantor, Chile) radiotelescopes. The observations, centered at  $\alpha_{\text{J2000}} = 17^{\text{h}}47^{\text{m}}22^{\text{s}}$  and  $\delta_{\text{J2000}} = -28^{\circ}21'27''$ , were made in position-switching mode, with the off position located at  $(-885'', +290'')$  with respect to G+0.693.

The IRAM 30m observations were obtained during 2019, as part of the projects 172–18 (PI Martín-Pintado), 018–19 and 133–19 (PI Rivilla). We have used the broad-band Eight MIXer Receiver (EMIR) and the FTS spectrometer (Fast Fourier Transform Spectrometer; Klein et al. 2012) to cover the frequency ranges 71.76–116.72 GHz, 124.77–175.5 GHz, 199.8–222.31 GHz, 223.32–238.29 GHz, 252.52–260.30 GHz, and 268.2–275.98 GHz, with a frequency resolution of  $\sim 800 \text{ kHz}$ , corresponding to  $0.9\text{--}3.3 \text{ km s}^{-1}$  at the observed frequencies. Pointing was checked every 1.5 hours, and focus was corrected at the beginning of the observations and after 4 hours. The HPBW of the telescope varies between  $8''9$  and  $34''3$ , across the covered frequency range.

The APEX observations were obtained during ten observing runs from July 11 to September 26 2021 in service mode, for a total of 23.4 hr as part of the project 0108.F-9308 (PI Rivilla). We used the NFLASH receiver, which allows the simultaneous observations of two sidebands, each one recorded by two spectrometer processors units (FFTS) of 4 GHz that overlap for 100 MHz, providing a total coverage of 7.9 GHz. We observed two different frequency setups centering the

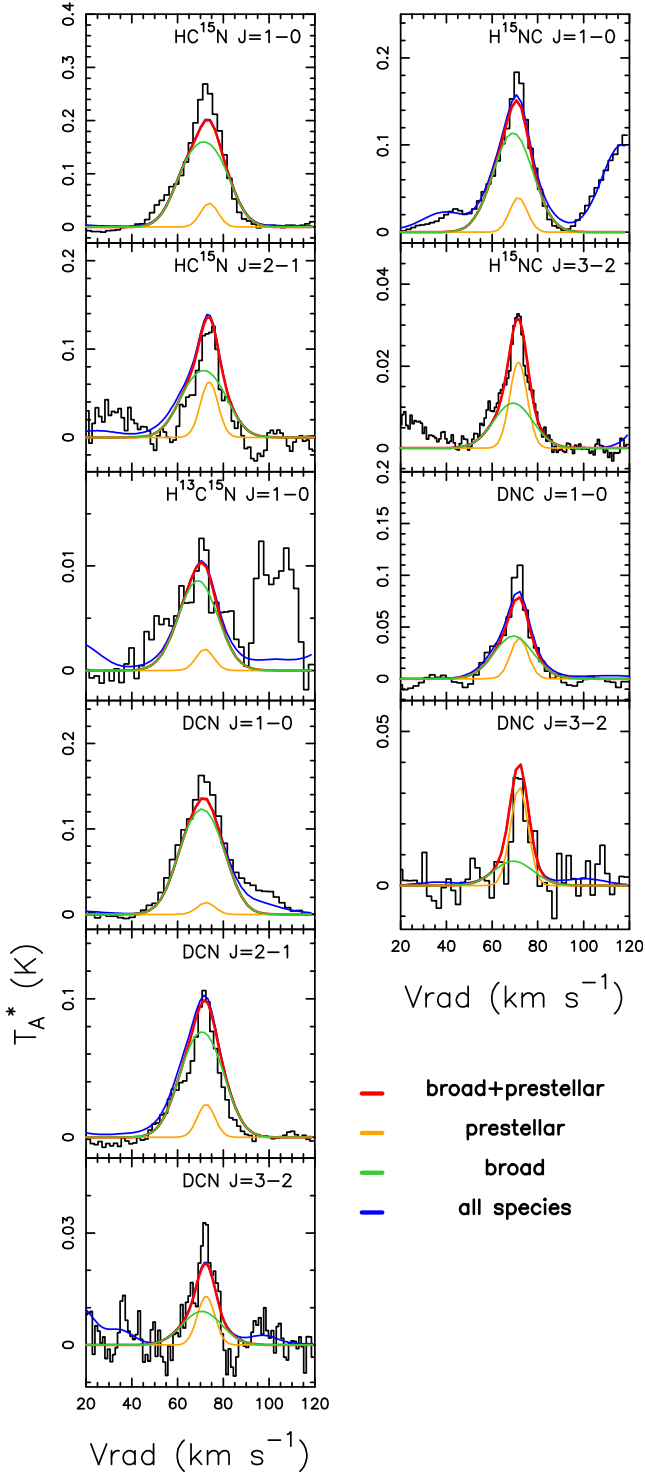


**Figure 1.** Observed transitions of the isotopologues of HCN (left) and HNC (right) studied in this work. The transition shown in each panel are indicated in the upper right. The orange line is the best LTE fit to the pre-stellar component, the green line is the best LTE fit to the broad gas component, and the red line is the sum of the components. The blue line indicates the total modelled line emission, including also the contribution of all molecular species previously identified in the survey (e.g. Rodríguez-Almeida et al. 2021a,b; Rivilla et al. 2021; Zeng et al. 2021).

upper sideband at 262.0 GHz and 262.3 GHz, respectively. The covered spectral ranges were 243.94–252.12 GHz and 260.18–268.37 GHz, with a spectral resolution of 0.244 MHz ( $\sim 0.3$  km s $^{-1}$  at 262 GHz). The spectra analysed in this work, which contain H $^{15}$ NC(3–2) and H $^{13}$ C $^{15}$ N(3–2), has been smoothed to  $\sim 800$  kHz ( $\sim 1.1$  km s $^{-1}$  at 266 GHz) to match the spectral resolution of the IRAM 30m observations. The precipitable water vapour (pwv) during the observations was 0.7–3.6 mm. Focus was performed at the beginning of each observing run, and pointing was checked every 1–2 hr. The HPBW varies between 23''2 and 25''6 at the observed frequency range.

The line intensity of the spectra was measured in antenna temperature  $T_A^*$  units since the molecular emission towards G+0.693 is extended over the beam (e.g. Zeng et al. 2020).

### 3. ANALYSIS AND RESULTS

We show the observed spectra of deuterated species of HCN, HNC, HCO $^+$  and N $_2$ H $^+$  together with the optically thin isotopologues ( $^{13}$ C,  $^{15}$ N,  $^{13}$ C $^{15}$ N, and  $^{18}$ O) of their hydrogen counterparts in Figs. 1 and 2. Spectra of transitions blended with other species are shown in Fig. A1. All the transitions targeted by our survey towards G+0.693 presented in this paper, which include the  $J=1-0$ ,  $J=2-1$ , and  $J=3-2$  transitions, are summarised in Table B1.

Most the observed lines profiles cannot be fitted with a single Gaussian component. The low lying energy transitions ( $J=1-0$  and  $J=2-1$ ) clearly show two components with different linewidths (broad and narrow), except for those of DCO $^+$  and N $_2$ D $^+(2-1)$ , and the  $J=3-2$  transitions of all molecules that mostly show the narrower component (see Figs. 1 and 2). As we discuss in Sect. 4, the broad component belongs to the G+0.693 warm and turbulent gas (hereafter "broad" component), usually observed in the emission from transitions of most of molecular species (e.g. Zeng et al. 2018; Rivilla et al. 2021). In contrast, the narrow component observed in the high- $J$  lines and for DCO $^+$  and N $_2$ D $^+$  reveals for the first time the presence of a less turbulent molecular gas (hereafter "pre-stellar" component).

We have used the SLIM (Spectral Line Identification and Modeling) tool within the MADCUBA package<sup>1</sup> (Martín et al. 2019) to identify and perform the multi-line profile fitting. SLIM generates a synthetic spectrum, assuming local thermodynamic equilibrium (LTE) con-

<sup>1</sup> Madrid Data Cube Analysis on ImageJ is a software developed at the Center of Astrobiology (CAB) in Madrid; <https://cab.inta-csic.es/madcuba/>.

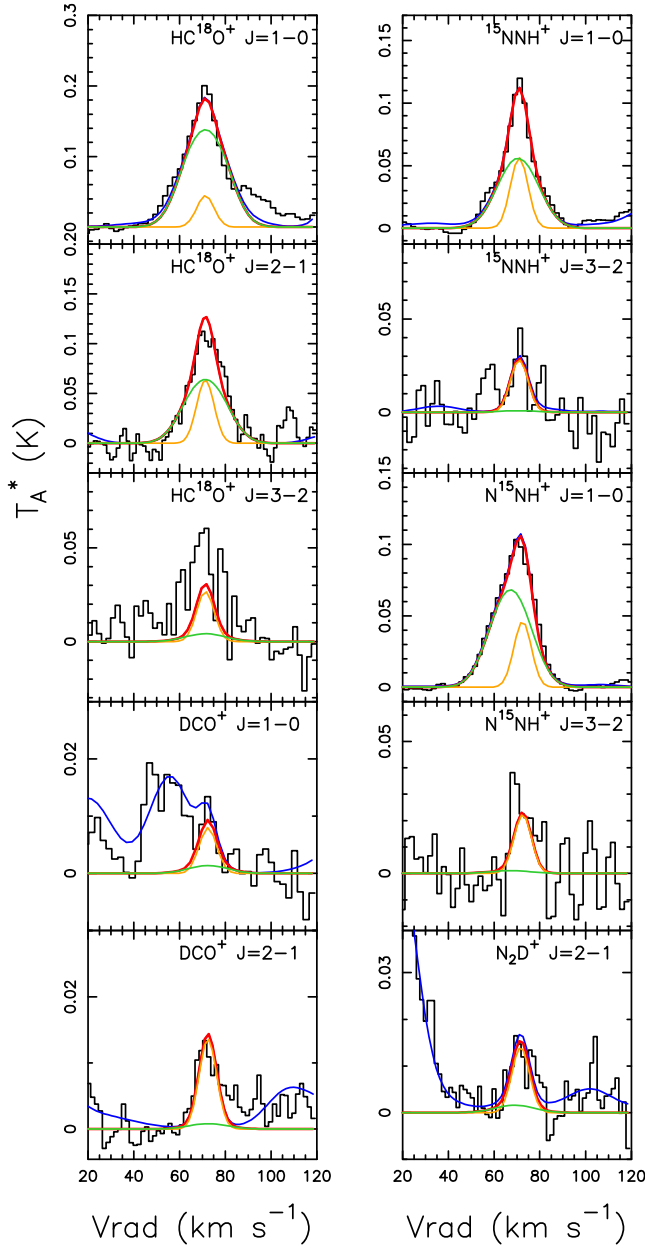


**Figure 2.** Observed transitions of the isotopologues of  $\text{HCO}^+$  (left) and  $\text{N}_2\text{H}^+$  (right) studied in this work. The transition shown in each panel are indicated in the upper right. The orange line is the best LTE fit to the pre-stellar component, the green line is the best LTE fit to the broad component, and the red line is the sum of the two profiles. The blue line indicates the total modelled line emission, including also the contribution of all molecular species previously identified in the survey (e.g. Rodríguez-Almeida et al. 2021a,b; Rivilla et al. 2021; Zeng et al. 2021).

ditions, and applies an algorithm (AUTOFIT) to find the best non-linear least-squares fit to the data. The free parameters to be fitted are the column density of the molecule,  $N$ , the excitation temperature,  $T_{\text{ex}}$ , the

peak velocity,  $v_{\text{LSR}}$ , and the full-width-half-maximum,  $FWHM$  (see details in Martín et al. 2019).

To perform the LTE line fitting we have only used the transitions that are not blended with emission from other species (see details in Table B1). The fit procedure requires a total of 8 free parameters to take into account the two velocity components for each molecular species. Thus, to help the fit to converge we have fixed for all the species the  $T_{\text{ex}}$  and the  $FWHM$  to the values as explained below. To define the best  $FWHM$  for the narrow component we have fitted a single Gaussian profile to the transitions for which this component clearly dominates, i.e.  $^{15}\text{NNH}^+$  and  $\text{N}^{15}\text{NH}^+(3-2)$ ,  $\text{DNC}(3-2)$ ,  $\text{N}_2\text{D}^+(2-1)$ ,  $\text{DCO}^+(1-0)$ , and  $(3-2)$ . The average  $FWHM$  derived for these transition is  $9 \pm 2 \text{ km s}^{-1}$ . Then, we have used the same procedure for the broad component using  $\text{HC}^{18}\text{O}^+(1-0)$ ,  $\text{DCN}(1-0)$ ,  $\text{H}^{15}\text{NC}(1-0)$ , and  $\text{HC}^{15}\text{N}(1-0)$ , obtaining an average  $FWHM$  of  $20 \pm 1 \text{ km s}^{-1}$ . Thus, we have used for the broad and the pre-stellar components linewidths of  $20 \text{ km s}^{-1}$  and  $9 \text{ km s}^{-1}$ , respectively, which reproduce well all the observed lines profiles for all molecules (Figs. 1 and 2).

To derive the  $T_{\text{ex}}$ , we have used  $\text{HC}^{18}\text{O}^+$ , because it is the only non D-bearing species with three detected transitions ( $J=1-0$ ,  $2-1$ , and  $3-2$ ) which appear unblended. The  $T_{\text{ex}}$  that better reproduce the three transitions (left panel of Fig. 2) are 7 K for the pre-stellar component and  $\sim 3$  K for the broad component. For  $\text{H}^{15}\text{NC}$  we find that the broad component will be better fitted with  $T_{\text{ex}}$  of  $4.3 \pm 0.1$  K. Given the possible uncertainties in the  $T_{\text{ex}}$  we used the values of 3 K and 7 K to fit the broad and pre-stellar components in other molecules, except for  $\text{DNC}$  for which we used the same  $T_{\text{ex}}$  derived from  $\text{H}^{15}\text{NC}$ . The difference in the  $T_{\text{ex}}$  clearly indicates that the pre-stellar component arises from higher density gas than the broad component with  $n \sim 10^4 \text{ cm}^{-3}$  (Zeng et al. 2020), but it only contributes with 10% to the total column density. This will be discussed in Sect. 4.

We applied MADCUBA-AUTOFIT, leaving free  $N$  and  $v_{\text{LSR}}$ , with the exception of  $\text{H}^{13}\text{C}^{15}\text{N}(3-2)$ , for which the best fit to the line profiles were obtained with  $v_{\text{LSR}}$  fixed to  $72 \text{ km s}^{-1}$  and to  $69 \text{ km s}^{-1}$  for the pre-stellar and the broad components, respectively (see Table 1). The AUTOFIT provides the best solution for the free parameters, and their associated errors. The  $v_{\text{LSR}}$  obtained from the different molecules are consistent with a redshifted pre-stellar component with respect to the broad component. We are confident that this component is not associated with foreground gas since it would present a different velocity than the bulk of dense gas observed towards the star-forming regions in the Sgr B2 cloud ( $\sim 50-70 \text{ km s}^{-1}$ , e.g. Goicoechea & Cernicharo

2002). We estimate that the total column density can be uncertain by up to 20% due to the absolute calibration errors.

The derived physical parameters are presented in Table 1, and the best LTE fits to the different line profiles are shown in Figures 1 and 2 with coloured solid lines. The orange line corresponds to the pre-stellar component fit, the green line shows the fit to the broad component, and the red line is the sum of the two profiles. The additional blue line also shows the contribution from other molecular species previously identified in the survey (e.g Zeng et al. 2018; Rivilla et al. 2021).

To compute the D/H ratios, the derived column density of  $^{13}\text{C}$ ,  $^{15}\text{N}$ , and  $^{18}\text{O}$  isotopologues have been converted to the column densities of the main isotopologues using the typical isotopic ratios found in the CMZ:  $^{12}\text{C}/^{13}\text{C}=20$  (Wilson & Rood 1994),  $^{14}\text{N}/^{15}\text{N}=900$  (Guesten & Ungerechts 1985), or  $^{16}\text{O}/^{18}\text{O}=250$  (Wilson & Rood 1994). The quoted errors in the D/H ratios also consider an additional 20% error due to the assumed isotopic ratios. The D/H ratios obtained for HCN and HNC range from  $\sim 3.6 \times 10^{-4}$  up to  $\sim 1.3 \times 10^{-3}$  taking into account both components (see Table 1 and Figure 3). For  $\text{HCO}^+$  and  $\text{N}_2\text{H}^+$ , the deuterated species were detected only in the pre-stellar component, giving D/H ratios  $> 10^{-4}$ . For the broad component, in contrast, we derived upper limits for the D/H ratios  $< 3.1 \times 10^{-5}$  and  $< 5.7 \times 10^{-5}$  for  $\text{HCO}^+$  and  $\text{N}_2\text{H}^+$ , respectively. The upper limits on the total column density of  $\text{DCO}^+$  and  $\text{N}_2\text{D}^+$  have been derived taking into account the  $3\sigma$  root-mean-square (*rms*) of the integrated intensity at the rest frequencies indicated in Table 1. While the deuteration fraction between the pre-stellar and broad components are  $\sim 0.4$  and  $\sim 3.3$  for HCN and HNC, respectively, it increases to  $\geq 30$  and  $\geq 4$  for  $\text{HCO}^+$  and  $\text{N}_2\text{H}^+$ , respectively. This clearly shows the large differences in the D fractionation for  $\text{HCO}^+$  and  $\text{N}_2\text{H}^+$  with respect to nitriles in both components.

We have also checked if the differences found in the isotopic compositions of the two components are still significant when considering different *FWHM* and  $T_{\text{ex}}$  than those used for the LTE fit. To do that, we have explored different values of these parameters for the two components and for which the fit converges. In particular, for the narrow component we have explored  $T_{\text{ex}}$  between 5 and 15 K, and for the broad component between 3 and 6 K. We have found that for the narrow component, the D/H ratios vary by factors of 1-1.8 and 1-3.4 with respect to those shown in Table 1 for HNC and  $\text{N}_2\text{H}^+$ , respectively, for the temperature ranges considered. For the broad component, the D/H ratio of HNC varies by factors 0.9-1.3, and the D/H upper limit

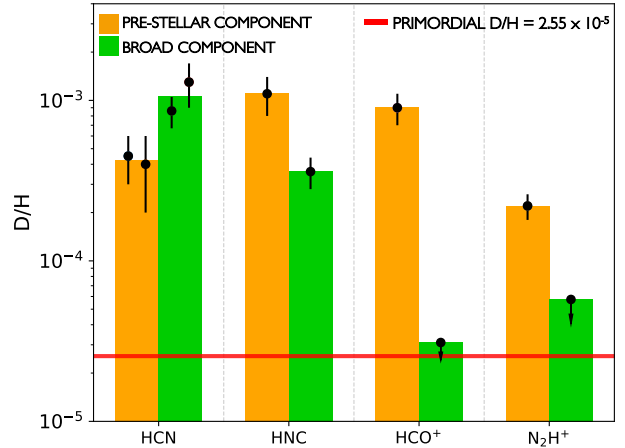


**Figure 3.** D/H ratios found for the different molecules, in the pre-stellar (orange) and broad (green) components. The red horizontal line indicate the primordial D/H value of  $(2.55 \pm 0.03) \times 10^{-5}$  (Zavarygin et al. 2018).

of  $\text{N}_2\text{H}^+$  varies by factors 0.4-1 with respect to those shown in Table 1. In the range of  $T_{\text{ex}}$  used, the deuteration fraction between the narrow and the broad component varies only between 3.3 and 4.3 for HNC, and between  $> 4$  and  $> 19$  for  $\text{N}_2\text{H}^+$ . Thus, the differences in the isotopic composition of the two components and between the different species are still significant despite the possible uncertainties in  $T_{\text{ex}}$ .

We have also explored the effects of changes in the *FWHM* between  $9 \text{ km s}^{-1}$  and  $11 \text{ km s}^{-1}$  for the narrow component and between  $15 \text{ km s}^{-1}$  and  $25 \text{ km s}^{-1}$  for the broad component. In this case, for the narrow component, the D/H ratios vary by factors of 1-1.45 and 1-1.2 with respect to those shown in Table 1 for HNC and  $\text{N}_2\text{H}^+$ , respectively, for the *FWHM* ranges considered. For the broad component, the D/H ratio of HNC varies by factors 1-1.14, and the D/H upper limit of  $\text{N}_2\text{H}^+$  varies by factors 1-1.25 with respect to those shown in Table 1. In the range of possible *FWHM*, the deuteration fraction between the narrow and the broad component varies between 3.3 and 4 for HNC, and between  $> 2$  and  $> 4$  for  $\text{N}_2\text{H}^+$ . Thus, we conclude that the differences in the isotopic composition of the two components and for the two species are still significant even assuming rather extremes values of line widths and  $T_{\text{ex}}$ .

#### 4. DISCUSSION AND CONCLUSIONS

The Sgr B2 cloud complex is one of the most active sites of star formation in our Galaxy. As already explained in Sect. 1, towards its densest part, this molecular cloud harbours three well-known massive star-forming clusters: Sgr B2(N) (in the north), Sgr B2(M) (in the centre), and Sgr B2(S) (in the south) that com-

**Table 1.** Results from the LTE fitting procedure.

Molecule	$FWHM$ ( $\text{km s}^{-1}$ )	$v_{\text{LSR}}$ ( $\text{km s}^{-1}$ )	$T_{\text{ex}}$ (K)	$N$ ( $\times 10^{12} \text{ cm}^{-2}$ )	D/H ( $\times 10^{-4}$ )
HCN					
DCN	9	$72.5 \pm 0.8$	7	$0.33 \pm 0.06$	
DCN	20	$70.7 \pm 0.3$	3	$39.8 \pm 1.4$	
$\text{HC}^{15}\text{N}$	9	$73.9 \pm 0.6$	7	$0.81 \pm 0.15$	$4.5 \pm 1.5$
$\text{HC}^{15}\text{N}$	20	$71.5 \pm 0.6$	3	$51 \pm 4$	$8.6 \pm 1.9$
$\text{H}^{13}\text{C}^{15}\text{N}$	9	72	7	$0.072 \pm 0.019$	$4 \pm 2$
$\text{H}^{13}\text{C}^{15}\text{N}$	20	69	3	$1.4 \pm 0.2$	$13 \pm 4$
HNC					
DNC	9	$71.9 \pm 0.5$	7	$0.83 \pm 0.11$	
DNC	20	$69.4 \pm 1.1$	4.3	$2.4 \pm 0.3$	
$\text{H}^{15}\text{NC}$	9	$71.55 \pm 0.14$	7	$0.84 \pm 0.04$	$11 \pm 3$
$\text{H}^{15}\text{NC}$	20	$69.22 \pm 0.16$	$4.3 \pm 0.1$	$7.48 \pm 0.16$	$3.6 \pm 0.8$
$\text{HCO}^+$					
$\text{DCO}^+$	9	$72.4 \pm 0.5$	7	$0.12 \pm 0.01$	
$\text{DCO}^+$	20	70	3	$\leq 0.2^a$	
$\text{HC}^{18}\text{O}^+$	9	$71.3 \pm 0.6$	7	$0.48 \pm 0.06$	$9 \pm 2$
$\text{HC}^{18}\text{O}^+$	20	$71.3 \pm 0.5$	3	$23.4 \pm 1.5$	$\leq 0.31$
$\text{N}_2\text{H}^+$					
$\text{N}_2\text{D}^+$	9	$71.7 \pm 0.8$	7	$0.15 \pm 0.02$	
$\text{N}_2\text{D}^+$	20	69	3	$\leq 0.5^b$	
$^{15}\text{NNH}^+$	9	$71.01 \pm 0.5$	7	$0.74 \pm 0.09$	$2.2 \pm 0.4$
$^{15}\text{NNH}^+$	28	$70.5 \pm 0.9$	3	$8.9 \pm 0.9$	$\leq 0.64$
$\text{N}^{15}\text{NH}^+$	9	$72.5 \pm 0.5$	7	$0.59 \pm 0.09$	$2.7 \pm 0.8$
$\text{N}^{15}\text{NH}^+$	20	$67.2 \pm 0.7$	3	$11.2 \pm 0.9$	$\leq 0.51$

NOTE—Parameters without errors are fixed in the fitting procedure, as explained in Sect. 3.

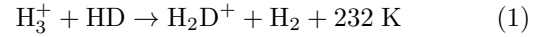
<sup>a</sup>Upper limit derived taking into account the *rms* of  $\sim 1.1$  mK at 144.083 GHz.

<sup>b</sup>Upper limit derived taking into account the *rms* of  $\sim 2.7$  mK at 154.22 GHz.

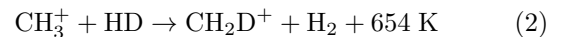
prise numerous compact and ultra-compact HII regions (e.g. Gaume et al. 1995; Schmiedeke et al. 2016; Ginsburg et al. 2018). However, the presence of filament-, arc- and shell-shaped dense gas likely produced by stellar feedback (Martín-Pintado et al. 1999), and of a large population of high-mass protostellar cores found by Ginsburg et al. (2018), indicate that star formation is not restricted to the central cloud region, but it is also taking place in the extended envelope of Sgr B2. Since Sgr B2(M) is considered to be more evolved than Sgr B2(N) and (S) (e.g. de Vicente et al. 2000; Ginsburg et al. 2018), star-forming activity may proceed sequentially from Sgr B2(M) and outwards, to continue towards

Sgr B2(N) in the north and Sgr B2(S) in the south. In the scenario of sequential star formation, it is expected that G+0.693 is in an earlier evolutionary phase since it is located northeast of Sgr B2(N).

Previous observations towards the quiescent clouds in the GC traced only the turbulent warm gas in a very turbulent component unable to form stars. Our observations of deuterated species reveal, for the first time, very low D/H ratios in  $\text{HCO}^+$  and  $\text{N}_2\text{H}^+$ , close to the cosmic value, for the turbulent broad component and the presence of a new narrow ( $FWHM$  of  $9 \text{ km s}^{-1}$ ) quiescent component, with high levels of deuteration in HCN, HNC,  $\text{HCO}^+$  and  $\text{N}_2\text{H}^+$  ( $\text{D}/\text{H} > 10^{-4}$ , see Fig. 3). This gas is clearly less turbulent (narrower  $FWHM$ ) than the surrounding gas (broad gas component with a  $FWHM$  of  $20 \text{ km s}^{-1}$ ), exhibiting similarly properties to those found in Galactic disc pre-stellar cores. The different degrees of D fractionation found in  $\text{HCO}^+$  and  $\text{N}_2\text{H}^+$  for both components indicates that the pre-stellar component should have a kinetic temperature  $T \leq 30 \text{ K}$ , smaller than the temperature of the broad component  $T > 100 \text{ K}$ . Indeed, at low kinetic temperatures, the reaction (Dalgarno & Lepp 1984)



efficiently produces  $\text{H}_2\text{D}^+$  which can react with  $\text{N}_2$ , CN, and CO, enhancing the abundances of  $\text{N}_2\text{D}^+$ , DCN, DNC and  $\text{DCO}^+$  to the observed values. The D/H ratios derived from HCN and HNC in both the broad and pre-stellar components are similar. This is in good agreement with the idea that DCN and DNC not only are formed at  $T < 30 \text{ K}$  as explained above, but also through additional high-temperature routes (see e.g. Roueff et al. 2013). Indeed, for high temperatures ( $T > 70\text{--}80 \text{ K}$ ) the reaction



starts to be more efficient than reaction (1). Then,  $\text{CH}_2\text{D}^+$  reacts with atomic N and initiates a chain of reactions that ends up with high deuterium fractionation in DCN and DNC ( $\text{D}/\text{H} > 10^{-4}$ , Roueff et al. 2007) and very low fractionation in  $\text{N}_2\text{D}^+$  ( $\text{D}/\text{H} < 3.1 \times 10^{-5}$ ), as observed for the broad warm component.  $\text{CH}_2\text{D}^+$ , reacting with O and CO, could also contribute to an efficient formation of  $\text{DCO}^+$  at high temperatures, as shown by Favre et al. (2015). However, these models show that these reactions are only efficient for the inner dense part of protoplanetary discs. Since we found for  $\text{HCO}^+$  a very low D fractionation ( $\text{D}/\text{H} < 3.1 \times 10^{-5}$ ) for the broad component, this suggests that such pathways are not efficient for the typical densities found in the GC ( $\sim 10^4 \text{ cm}^{-3}$ ).

The D/H values derived for the pre-stellar component towards G+0.693 are similar to previous observations of several deuterated complex organic molecules (COMs) towards the GC star-forming hot core Sgr B2(N2) (D/H from  $5 \times 10^{-4}$  to  $4 \times 10^{-3}$ , Belloche et al. 2016), of DCN towards the star-forming  $50 \text{ km s}^{-1}$  cloud in the Sgr A\* region (D/H =  $4 \times 10^{-4}$ , Lubowich et al. 2000), and of HDO towards Sgr B2 (D/H from  $5 \times 10^{-4}$  to  $10^{-3}$ , Comito et al. 2003).

Previous measurements in the GC showed much larger D/H ratio than the primordial value, indicating a large (20–200) degree of chemical fractionation. Jacq et al. (1999); Lubowich et al. (2000) and Polehampton et al. (2002), claimed, through chemical modelling, that the atomic D/H ratios may be up to  $\sim 100$  times lower in the Galactic Centre region than in the local ISM because of stellar processing in the interior of stars. Our measured upper limit of the D/H ratio, for the first time close to the cosmic D/H ratio, is still consistent with this claim, but the large differences in the degree of fractionation in different molecules suggest that model predictions need to be considered with caution. Further observations of DCO<sup>+</sup> and N<sub>2</sub>D<sup>+</sup> towards other quiescent molecular clouds in the GC, will firmly establish the degree of processing of the material in this region of the Galaxy.

Additional support for the presence of a multi-phase ISM in the GC comes from the excitation temperature derived for both components in Table 1 which translate to very different H<sub>2</sub> densities. Using the non-LTE molecular radiative transfer model RADEX (van der Tak et al. 2007) we derive for the warm broad component, assuming a kinetic temperature of 100 K and a *FWHM* of  $20 \text{ km s}^{-1}$ , that the derived  $T_{\text{ex}}$  of 3–4 K translate to H<sub>2</sub> densities of  $0.3\text{--}3 \times 10^4 \text{ cm}^{-3}$ . For the cold pre-stellar component, assuming kinetic temperatures of 20–30 K and a *FWHM* of  $9 \text{ km s}^{-1}$ , with  $T_{\text{ex}}$  of 7 K the required H<sub>2</sub> densities increase by at least one order of magnitude to  $0.05\text{--}1 \times 10^6 \text{ cm}^{-3}$ . It should be noted that the densities obtained for the narrow component are a factor from 5 up to 30 larger than for the broad component of the molecular species studied in this work. This confirms that the two components are tracing different phases of molecular gas. Moreover, higher temperatures (e.g. 100 K) and lower densities (e.g.  $10^4 \text{ cm}^{-3}$ ), similar to those of the broad component, are not consistent neither with the D/H ratios obtained, nor with the LTE, and the non-LTE analysis performed for the narrow component, since the predicted line intensities are one order of magnitude lower than observed. The large difference in the

linewidth, the kinetic temperature and the density from the warm broad component to the pre-stellar component suggests that a substantial fraction (10% in column density) of gas in the GC has the conditions to form the new generation of stars. This denser gas component was likely form through the cloud-cloud collisions known to occur in the Sgr B2 complex (Fukui et al. 2021).

To conclude, in this Letter we have shown that combined observations of the degree of deuteration of different molecules, such as N<sub>2</sub>H<sup>+</sup> and HCO<sup>+</sup>, can be used to reveal the different gas components in the line of sight of the CMZ, allowing to identify denser gas that is on the verge of gravitational collapse and which will host future protostars. A study of another similar sources in the CMZ could provide information on the ubiquity of the multi-phase environment in the Galactic centre. Moreover, the CMZ might be used as a template for the nuclei of other galaxies since some starburst galaxies like NGC 253, M82 and IC 342 contain gas with average densities and gas temperatures similar to those found in the CMZ for the broad warm component (e.g. Aladro et al. 2011). Thus, observations of deuterated molecules in nearby galaxies could be crucial to identify and investigate the earliest evolutionary stages of extragalactic protoclusters, and to understand the full star-formation sequence in external galaxies.

#### ACKNOWLEDGMENTS

We are grateful to the IRAM 30m telescope staff for their help during the different observing runs, and the APEX staff for conducting the observations. IRAM is supported by the National Institute for Universe Sciences and Astronomy/National Center for Scientific Research (France), Max Planck Society for the Advancement of Science (Germany), and the National Geographic Institute (IGN) (Spain). APEX is a collaboration between the Max-Planck-Institut fuer Radioastronomie, the European Southern Observatory, and the Onsala Observatory. L. C. and V. M.R. acknowledge support from the Comunidad de Madrid through the Atracción de Talento Investigador Senior Grant (COOL: Cosmic Origins Of Life; 2019-T1/TIC-15379). J.M.-P. and I.J.-S. have received partial support from the Spanish State Research Agency through project number PID2019-105552RB-C41.

*Facilities:* IRAM 30m, APEX

*Software:* MADCUBA

#### APPENDIX

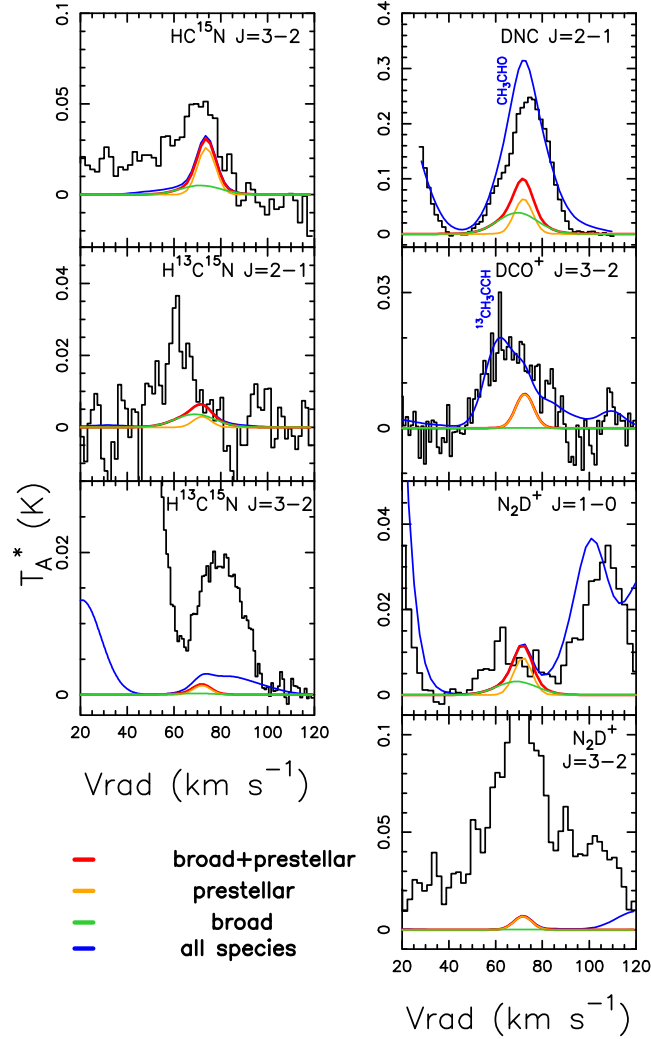


**Figure A1.** Observed transitions that are blended with other species. The molecule and transition shown in each panel are indicated in the upper right. Blending species are indicated in blue when known. The orange line is the best LTE fit to the pre-stellar component, the green line is the best LTE fit to the broad gas component, and the red line is the sum of the components. The blue line indicates the total modelled line emission, including also the contribution of all molecular species previously identified in the survey (e.g. [Rodríguez-Almeida et al. 2021a,b](#); [Rivilla et al. 2021](#); [Zeng et al. 2021](#)).

#### A. BLENDED TRANSITIONS

Figure [A1](#) shows the transitions present in the spectral setup but not used for the analysis because they appear blended with other species.

#### B. SPECTROSCOPIC INFORMATION

The transitions of the molecules studied in this work were taken from the catalogues and spectroscopic works listed in [Table B1](#). Moreover, [Table B1](#) indicates possible blending with other species and the telescope used for the observation.

#### REFERENCES

- |   |  |
|---|--|
| <p>Aladro, R., Martín-Pintado, J., Martín, S., Mauersberger, R., &amp; Bayet, E. 2011, <i>A&amp;A</i>, 525, A89,<br/>doi: <a href="https://doi.org/10.1051/0004-6361/201014090">10.1051/0004-6361/201014090</a></p> | <p>Amano, T., Hirao, T., &amp; Takano, J. 2005, <i>Journal of Molecular Spectroscopy</i>, 234, 170,<br/>doi: <a href="https://doi.org/10.1016/j.jms.2005.09.004">10.1016/j.jms.2005.09.004</a></p> |
|---|--|



**Table B1.** Transitions of the molecules present in the G+0.693 dataset (Sect. 2). The first column indicates the molecule for which the transitions are listed. The second and third columns show the rotational transitions and the related frequencies, respectively.  $\log I$  is the base 10 logarithm of the integrated intensity at 300 K and  $E_{\text{up}}$  is the energy of the upper level. Columns 6–8 contain the spectroscopic information for the molecules studied in this work. The last column indicate whether the transition is blended or not with other molecular species.

Molecule	Transition ( $J'-J$ )	Frequency (GHz)	$\log I$ ( $\text{nm}^2 \text{ MHz}$ )	$E_{\text{up}}$ (K)	Catalogue/Entry/Date	Line list reference	Dipole moment reference	Blended
HC <sup>15</sup> N	1–0	86.0550	-2.5525	4.1	CDMS/28506/Dec. 2017	(1), (2)	(3)	No
HC <sup>15</sup> N	2–1	172.1080	-1.6584	12.4	–	–	–	No
HC <sup>15</sup> N	3–2	258.1570	-1.1450	24.8	–	–	–	Yes <sup>a</sup>
H <sup>13</sup> C <sup>15</sup> N	1–0	83.7276	-2.5875	4.0	CDMS/29512/Dec. 2006	(1)	(3)	No
H <sup>13</sup> C <sup>15</sup> N	2–1	167.4533	-1.6931	12.1	–	–	–	Yes <sup>a</sup>
H <sup>13</sup> C <sup>15</sup> N	3–2 <sup>b</sup>	251.1752	-1.1794	24.1	–	–	–	Yes <sup>a</sup>
DCN	1–0	72.4147	-2.7990	3.5	CDMS/28509/Apr. 2006	(4), (5)	(6)	No
DCN	2–1	144.8280	-1.9034	10.4	–	–	–	No
DCN	3–2	217.2385	-1.3877	20.9	–	–	–	No
H <sup>15</sup> NC	1–0	88.8657	-2.5690	4.3	JPL/28006/Dec. 1979	(7), (8)	(9)	No
H <sup>15</sup> NC	3–2 <sup>b</sup>	266.5878	-1.1624	25.6	–	–	–	No
DNC	1–0	76.3057	-2.6611	3.7	CDMS/28508/Sep. 2009	(10), (11), (12)	(9)	No
DNC	2–1	152.6097	-1.7660	11.0	–	–	–	Yes <sup>c</sup>
DNC	3–2	228.9105	-1.2510	22.0	–	–	–	No
HC <sup>18</sup> O <sup>+</sup>	1–0	85.1622	-2.3049	4.1	CDMS/31506/Dec. 2004	(13), (14)	(15)	No
HC <sup>18</sup> O <sup>+</sup>	2–1	170.3226	-1.4107	12.3	–	–	–	No
HC <sup>18</sup> O <sup>+</sup>	3–2	255.4794	-0.8972	24.5	–	–	–	No
DCO <sup>+</sup>	1–0	72.0393	-2.5223	3.5	CDMS/30510/Sep. 2009	(10), (16), (17)	(15)	No
DCO <sup>+</sup>	2–1	144.0773	-1.6267	10.4	–	–	–	No
DCO <sup>+</sup>	3–2	216.1126	-1.1110	20.8	–	–	–	Yes <sup>d</sup>
<sup>15</sup> NNH <sup>+</sup>	1–0	90.2638	-2.3485	4.3	CDMS/30507/Mar. 2009	(18)	(19)	No
<sup>15</sup> NNH <sup>+</sup>	3–2	270.7836	-0.9422	26.0	–	–	–	No
N <sup>15</sup> NH <sup>+</sup>	1–0	91.2057	-2.3350	4.4	CDMS/30508/Mar. 2009	(18)	(19)	No
N <sup>15</sup> NH <sup>+</sup>	3–2	273.6090	-0.9290	26.3	–	–	–	No
N <sub>2</sub> D <sup>+</sup>	1–0	77.1092	-2.5531	3.7	CDMS/30509/Mar. 2009	(20), (21), (22)	(19)	Yes <sup>a</sup>
N <sub>2</sub> D <sup>+</sup>	2–1	154.2170	-1.6581	11.1	–	–	–	No
N <sub>2</sub> D <sup>+</sup>	3–2	231.3218	-1.1432	22.2	–	–	–	Yes <sup>a</sup>

NOTE—All the transitions have been observed with the IRAM 30m, except when specified with a note.

**References**—(1) Fuchs et al. (2004); (2) Cazzoli et al. (2005); (3) Ebenstein & Muentner (1984); (4) Brünken et al. (2004); (5) Möllmann et al. (2002); (6) DeLeon & Muentner (1984); (7) Creswell et al. (1976); (8) Pearson et al. (1976); (9) Blackman et al. (1976); (10) van der Tak et al. (2009); (11) Bechtel et al. (2006); (12) Okabayashi & Tanimoto (1993); (13) Plummer et al. (1983); (14) Schmid-Burgk et al. (2004); (15) Botschwina et al. (1993); (16) Caselli & Dore (2005); (17) Lattanzi et al. (2007); (18) Dore et al. (2009); (19) Havenith et al. (1990); (20) Pagani et al. (2009); (21) Dore et al. (2004); (22) Amano et al. (2005).

<sup>a</sup>Blended with unidentified molecular species.

<sup>b</sup>Transition observed with APEX.

<sup>c</sup>Blended with CH<sub>3</sub>CHO at 152.607 GHz.

<sup>d</sup>Blended with <sup>13</sup>CH<sub>3</sub>CCH at 216.115 GHz and 216.119 GHz.

- Barnes, A. T., Longmore, S. N., Battersby, C., et al. 2017, *MNRAS*, 469, 2263, doi: [10.1093/mnras/stx941](https://doi.org/10.1093/mnras/stx941)
- Bechtel, H. A., Steeves, A. H., & Field, R. W. 2006, *ApJL*, 649, L53, doi: [10.1086/508272](https://doi.org/10.1086/508272)
- Belloche, A., Müller, H. S. P., Garrod, R. T., & Menten, K. M. 2016, *A&A*, 587, A91, doi: [10.1051/0004-6361/201527268](https://doi.org/10.1051/0004-6361/201527268)
- Blackman, G. L., Brown, R. D., Godfrey, P. D., & Gunn, H. I. 1976, *Nature*, 261, 395, doi: [10.1038/261395a0](https://doi.org/10.1038/261395a0)
- Botschwina, P., Horn, M., Flügge, J., & Seeger, S. 1993, *J. Chem. Soc., Faraday Trans.*, 89, 2219, doi: [10.1039/FT9938902219](https://doi.org/10.1039/FT9938902219)
- Brünken, S., Fuchs, U., Lewen, F., et al. 2004, *Journal of Molecular Spectroscopy*, 225, 152, doi: [10.1016/j.jms.2004.02.021](https://doi.org/10.1016/j.jms.2004.02.021)
- Caselli, P., & Dore, L. 2005, *A&A*, 433, 1145, doi: [10.1051/0004-6361:20042118](https://doi.org/10.1051/0004-6361:20042118)
- Caselli, P., Vastel, C., Ceccarelli, C., et al. 2008, *A&A*, 492, 703, doi: [10.1051/0004-6361:20079009](https://doi.org/10.1051/0004-6361:20079009)
- Cazzoli, G., Puzzarini, C., & Gauss, J. 2005, *ApJS*, 159, 181, doi: [10.1086/430209](https://doi.org/10.1086/430209)
- Comito, C., Schilke, P., Gerin, M., et al. 2003, *A&A*, 402, 635, doi: [10.1051/0004-6361:20030293](https://doi.org/10.1051/0004-6361:20030293)
- Crapsi, A., Caselli, P., Walmsley, C. M., et al. 2005, *ApJ*, 619, 379, doi: [10.1086/426472](https://doi.org/10.1086/426472)
- Creswell, R. A., Pearson, E. F., Winnewisser, M., & Winnewisser, G. 1976, *Zeitschrift Naturforschung Teil A*, 31, 221, doi: [10.1515/zna-1976-3-401](https://doi.org/10.1515/zna-1976-3-401)
- Dalgarno, A., & Lepp, S. 1984, *ApJL*, 287, L47, doi: [10.1086/184395](https://doi.org/10.1086/184395)
- de Vicente, P., Martín-Pintado, J., Neri, R., & Colom, P. 2000, *A&A*, 361, 1058, <https://arxiv.org/abs/astro-ph/0009195>
- DeLeon, R. L., & Muentner, J. S. 1984, *JChPh*, 80, 3992, doi: [10.1063/1.447270](https://doi.org/10.1063/1.447270)
- Dore, L., Bizzocchi, L., Degli Esposti, C., & Tinti, F. 2009, *A&A*, 496, 275, doi: [10.1051/0004-6361/200811235](https://doi.org/10.1051/0004-6361/200811235)
- Dore, L., Caselli, P., Beninati, S., et al. 2004, *A&A*, 413, 1177, doi: [10.1051/0004-6361:20034025](https://doi.org/10.1051/0004-6361:20034025)
- Ebenstein, W. L., & Muentner, J. S. 1984, *JChPh*, 80, 3989, doi: [10.1063/1.447269](https://doi.org/10.1063/1.447269)
- Emprechtinger, M., Caselli, P., Volgenau, N. H., Stutzki, J., & Wiedner, M. C. 2009, *A&A*, 493, 89, doi: [10.1051/0004-6361:200810324](https://doi.org/10.1051/0004-6361:200810324)
- Favre, C., Bergin, E. A., Cleaves, L. I., et al. 2015, *ApJL*, 802, L23, doi: [10.1088/2041-8205/802/2/L23](https://doi.org/10.1088/2041-8205/802/2/L23)
- Fontani, F., Palau, A., Caselli, P., et al. 2011, *A&A*, 529, L7, doi: [10.1051/0004-6361/201116631](https://doi.org/10.1051/0004-6361/201116631)
- Fuchs, U., Bruenken, S., Fuchs, G. W., et al. 2004, *Zeitschrift Naturforschung Teil A*, 59, 861, doi: [10.1515/zna-2004-1123](https://doi.org/10.1515/zna-2004-1123)
- Fukui, Y., Habe, A., Inoue, T., Enokiya, R., & Tachihara, K. 2021, *PASJ*, 73, S1, doi: [10.1093/pasj/psaa103](https://doi.org/10.1093/pasj/psaa103)
- Gaume, R. A., Claussen, M. J., de Pree, C. G., Goss, W. M., & Mehringer, D. M. 1995, *ApJ*, 449, 663, doi: [10.1086/176087](https://doi.org/10.1086/176087)
- Ginsburg, A., Henkel, C., Ao, Y., et al. 2016, *A&A*, 586, A50, doi: [10.1051/0004-6361/201526100](https://doi.org/10.1051/0004-6361/201526100)
- Ginsburg, A., Bally, J., Barnes, A., et al. 2018, *ApJ*, 853, 171, doi: [10.3847/1538-4357/aaa6d4](https://doi.org/10.3847/1538-4357/aaa6d4)
- Goicoechea, J. R., & Cernicharo, J. 2002, *ApJL*, 576, L77, doi: [10.1086/343062](https://doi.org/10.1086/343062)
- Guesten, R., & Ungerechts, H. 1985, *A&A*, 145, 241
- Havenith, M., Zwart, E., Leo Meerts, W., & Ter Meulen, J. J. 1990, *JChPh*, 93, 8446, doi: [10.1063/1.459282](https://doi.org/10.1063/1.459282)
- Huettemeister, S., Wilson, T. L., Bania, T. M., & Martín-Pintado, J. 1993, *A&A*, 280, 255
- Jacq, T., Baudry, A., Walmsley, C. M., & Caselli, P. 1999, *A&A*, 347, 957
- Jiménez-Serra, I., Martín-Pintado, J., Rivilla, V. M., et al. 2020, *Astrobiology*, 20, 1048, doi: [10.1089/ast.2019.2125](https://doi.org/10.1089/ast.2019.2125)
- Klein, B., Hochgürtel, S., Krämer, I., et al. 2012, *Astronomy and Astrophysics*, 542, L3, doi: [10.1051/0004-6361/201218864](https://doi.org/10.1051/0004-6361/201218864)
- Krieger, N., Ott, J., Beuther, H., et al. 2017, *ApJ*, 850, 77, doi: [10.3847/1538-4357/aa951c](https://doi.org/10.3847/1538-4357/aa951c)
- Lattanzi, V., Walters, A., Drouin, B. J., & Pearson, J. C. 2007, *ApJ*, 662, 771, doi: [10.1086/517602](https://doi.org/10.1086/517602)
- Longmore, S. N., Rathborne, J., Bastian, N., et al. 2012, *ApJ*, 746, 117, doi: [10.1088/0004-637X/746/2/117](https://doi.org/10.1088/0004-637X/746/2/117)
- Longmore, S. N., Bally, J., Testi, L., et al. 2013, *MNRAS*, 429, 987, doi: [10.1093/mnras/sts376](https://doi.org/10.1093/mnras/sts376)
- Lubowich, D. A., Pasachoff, J. M., Balonek, T. J., et al. 2000, *Nature*, 405, 1025, doi: [10.1038/35016506](https://doi.org/10.1038/35016506)
- Martín, S., Martín-Pintado, J., Blanco-Sánchez, C., et al. 2019, *A&A*, 631, A159, doi: [10.1051/0004-6361/201936144](https://doi.org/10.1051/0004-6361/201936144)
- Martín, S., Requena-Torres, M. A., Martín-Pintado, J., & Mauersberger, R. 2008, *ApJ*, 678, 245, doi: [10.1086/533409](https://doi.org/10.1086/533409)
- Martín-Pintado, J., Gaume, R. A., Rodríguez-Fernández, N., de Vicente, P., & Wilson, T. L. 1999, *ApJ*, 519, 667, doi: [10.1086/307399](https://doi.org/10.1086/307399)
- Möllmann, E., Maki, A. G., Winnewisser, M., Winnewisser, B. P., & Quapp, W. 2002, *Journal of Molecular Spectroscopy*, 212, 22, doi: [10.1006/jmsp.2001.8519](https://doi.org/10.1006/jmsp.2001.8519)
- Morris, M., & Serabyn, E. 1996, *ARA&A*, 34, 645, doi: [10.1146/annurev.astro.34.1.645](https://doi.org/10.1146/annurev.astro.34.1.645)

- Okabayashi, T., & Tanimoto, M. 1993, *JChPh*, 99, 3268, doi: [10.1063/1.465135](https://doi.org/10.1063/1.465135)
- Pagani, L., Daniel, F., & Dubernet, M. L. 2009, *A&A*, 494, 719, doi: [10.1051/0004-6361:200810570](https://doi.org/10.1051/0004-6361:200810570)
- Pearson, E. F., Creswell, R. A., Winnewisser, M., & Winnewisser, G. 1976, *Zeitschrift Naturforschung Teil A*, 31, 1394, doi: [10.1515/zna-1976-1119](https://doi.org/10.1515/zna-1976-1119)
- Plummer, G. M., Herbst, E., & De Lucia, F. C. 1983, *ApJL*, 270, L99, doi: [10.1086/184078](https://doi.org/10.1086/184078)
- Polehampton, E. T., Baluteau, J. P., Ceccarelli, C., Swinyard, B. M., & Caux, E. 2002, *A&A*, 388, L44, doi: [10.1051/0004-6361:20020630](https://doi.org/10.1051/0004-6361:20020630)
- Requena-Torres, M. A., Martín-Pintado, J., Rodríguez-Franco, A., et al. 2006, *A&A*, 455, 971, doi: [10.1051/0004-6361:20065190](https://doi.org/10.1051/0004-6361:20065190)
- Rivilla, V. M., Martín-Pintado, J., Jiménez-Serra, I., et al. 2019, *MNRAS*, 483, L114, doi: [10.1093/mnrasl/sly228](https://doi.org/10.1093/mnrasl/sly228)
- . 2020, *ApJL*, 899, L28, doi: [10.3847/2041-8213/abac55](https://doi.org/10.3847/2041-8213/abac55)
- Rivilla, V. M., Jiménez-Serra, I., Martín-Pintado, J., et al. 2021, *Proceedings of the National Academy of Sciences*, 118, doi: [10.1073/pnas.2101314118](https://doi.org/10.1073/pnas.2101314118)
- Rodríguez-Almeida, L. F., Rivilla, V. M., Jiménez-Serra, I., et al. 2021a, *A&A*, 654, L1, doi: [10.1051/0004-6361/202141989](https://doi.org/10.1051/0004-6361/202141989)
- Rodríguez-Almeida, L. F., Jiménez-Serra, I., Rivilla, V. M., et al. 2021b, *ApJL*, 912, L11, doi: [10.3847/2041-8213/abf7cb](https://doi.org/10.3847/2041-8213/abf7cb)
- Roueff, E., Gerin, M., Lis, D. C., et al. 2013, *Journal of Physical Chemistry A*, 117, 9959, doi: [10.1021/jp400119a](https://doi.org/10.1021/jp400119a)
- Roueff, E., Parise, B., & Herbst, E. 2007, *A&A*, 464, 245, doi: [10.1051/0004-6361:20066531](https://doi.org/10.1051/0004-6361:20066531)
- Schmid-Burgk, J., Muders, D., Müller, H. S. P., & Brupbacher-Gatehouse, B. 2004, *A&A*, 419, 949, doi: [10.1051/0004-6361:20035589](https://doi.org/10.1051/0004-6361:20035589)
- Schmiedeke, A., Schilke, P., Möller, T., et al. 2016, *A&A*, 588, A143, doi: [10.1051/0004-6361/201527311](https://doi.org/10.1051/0004-6361/201527311)
- van der Tak, F. F. S., Black, J. H., Schöier, F. L., Jansen, D. J., & van Dishoeck, E. F. 2007, *A&A*, 468, 627, doi: [10.1051/0004-6361:20066820](https://doi.org/10.1051/0004-6361:20066820)
- van der Tak, F. F. S., Müller, H. S. P., Harding, M. E., & Gauss, J. 2009, *A&A*, 507, 347, doi: [10.1051/0004-6361/200912912](https://doi.org/10.1051/0004-6361/200912912)
- Wilson, T. L., & Rood, R. 1994, *ARA&A*, 32, 191, doi: [10.1146/annurev.aa.32.090194.001203](https://doi.org/10.1146/annurev.aa.32.090194.001203)
- Zavarygin, E. O., Webb, J. K., Dumont, V., & Riemer-Sørensen, S. 2018, *MNRAS*, 477, 5536, doi: [10.1093/mnras/sty1003](https://doi.org/10.1093/mnras/sty1003)
- Zeng, S., Jiménez-Serra, I., Rivilla, V. M., et al. 2018, *MNRAS*, 478, 2962, doi: [10.1093/mnras/sty1174](https://doi.org/10.1093/mnras/sty1174)
- Zeng, S., Zhang, Q., Jiménez-Serra, I., et al. 2020, *MNRAS*, 497, 4896, doi: [10.1093/mnras/staa2187](https://doi.org/10.1093/mnras/staa2187)
- Zeng, S., Jiménez-Serra, I., Rivilla, V. M., et al. 2021, *ApJL*, 920, L27, doi: [10.3847/2041-8213/ac2c7e](https://doi.org/10.3847/2041-8213/ac2c7e)